Supplementary Information (SI) for Chemical Communications.
This journal is © The Royal Society of Chemistry 2024

3D carbon skeleton/MOFs derivatives for efficient electromagnetic absorption and corrosion resistance

Song Chen[a,1], Yanwen Ji[a,1], Jinning Ke[a], Jie Zhou[a,*], Mengyu Zhang[a], Xiuxia Meng[a], Wenjie Hou[b,c,*], Dong Liu[a,*]

[a]School of Chemistry and Chemical Engineering, Shandong University of Technology, Zibo 255049, China.

[b]Institute of Fundamental and Frontier Sciences, University of Electronic Science and Technology of China, Chengdu 610054, China.

[c]Taizhou Key Laboratory of Minimally Invasive Interventional Therapy & Artificial Intelligence, Taizhou Campus of Zhejiang Cancer Hospital (Taizhou Cancer Hospital), Taizhou, Zhejiang 317502, China.

Emails: tjuzhoujie@163.com (J. Zhou), byhhwj@163.com (W.J. Hou), liu_dong@sdut.edu.cn (D. Liu)

[1]These authors contributed equally to this work.

1. Experimental section

1.1. Materials

Chitosan, Nacl and acetic acid (≥99.5%) were provided by Shanghai Adamas Reagent Co., Ltd. zinc nitrate hexahydrate ($Zn(NO_3)_2·6H_2O$), cobaltous nitrate hexahydrate ($Co(NO_3)_2·6H_2O$) , 2-methylimidazole and methyl alcohol (≥99.5%) were supplied by Shanghai Sinopharm Chemical Reagent Co., LTD.

1.2. Preparation of porous carbon skeleton

Firstly, 1.0 g chitosan was added to 50 mL deionized water and 0.5 mL acetic acid solution and with stirring for 30 min. Next, 4.0 g NaCl was also dispersed into the mixed solution and stirred for 24 h to obtain a white flocculent. The precursor was obtained by filtering and freeze-drying. These white flocculent was filtered, and after lyophilization, the products were annealed for 2 h at 800 °C in a nitrogen atmosphere to acquire the carbon skeleton.

1.3. Synthesis of the CS/ZIF-8 and CS/ZIF-67.

To obtain CS/ZIF-8, 1.04 g $Zn(NO_3)_2·6H_2O$ and 0.1 g carbon skeleton were added to 50 ml methanol then mixed with 0.58g 2-methylimidazole dissolved in 50 mL methanol, stirring for 90 min. After centrifugation and washing with methanol several times, the CS/ZIF-8 was obtained by drying under vacuum conditions at 60℃.

1.4 Characterization

Detailed examination of morphology and composition changes was carried out utilizing scanning electron microscopy (SEM, FEI Quanta 250) and transmission electron microscopy (TEM) integrated. Phase identification and crystal structure were determined through powder X-ray diffraction (XRD) analysis performed by a Bruker D8 Advance instrument. To analyze the molecular structure and atomic valence, Raman spectroscopy (WJGS-034 spectrometer) and X-ray photoelectron spectroscopy (XPS, ESCALAB 250Xi). Electromagnetic parameters were assessed using a vector network analyzer (VNA, Agilent PNA N5234A). The sample, mixed with paraffin in a mass ratio of 4:6, was pressed into a cylindrical shape (Φ_{in} = 3.04 mm, Φ_{out} = 7.00 mm) for testing within the frequency range of 2–18 GHz.

The corrosion resistance of the sample was evaluated in 3.5 wt% NaCl solution with different conditions (acidic, neutral, and alkaline) at room temperature using the three-electrode system integrated into a CHI660E electrochemical workstation. Various electrochemical techniques, including open circuit potential (OCP), electrochemical impedance spectroscopy (EIS), and potential polarization curves, were employed to comprehensively analyze the corrosion behavior. The reference electrode selected for the experiment was an Ag|AgCl (saturated KCl) reference electrode, while Pt foil was utilized as the counter electrode. Employing a glassy carbon electrode with a diameter of 4 mm as the working electrode, the solution consisting of the absorbent (5 mg) and 5 wt% Nafion solution (50 μL) was dispersed in 1000 μL of ethanol, followed by sonication for 30 min to form the mixed solution.

1.5 Electromagnetic absorption calculation

In accordance with transmission theory, the RL values were calculated as follows

$$Z_{in} = Z_0\sqrt{\mu_r/\varepsilon_r}\tanh\left(j2\pi fd/c\sqrt{\mu_r\varepsilon_r}\right) \tag{1}$$

$$RL(dB) = 20\lg\left|(Z_{in} - Z_0)/(Z_{in} + Z_0)\right| \tag{2}$$

where the input impedance (Z_{in}) and air impedance (Z_0) are normalized, with due consideration given to the complex permeability (μ_r) and dielectric constant (ε_r). Additionally, variables such as frequency (f), matching thickness (d), and the speed of light (c) are employed in the analysis.

$$\varepsilon' = \varepsilon_\infty + \frac{\varepsilon_s - \varepsilon_\infty}{1+\omega^2\tau^2} \tag{3}$$

$$\varepsilon'' = \frac{\varepsilon_s - \varepsilon_\infty}{1+\omega^2\tau^2}\omega\tau + \frac{\sigma}{\omega\varepsilon_0} \tag{4}$$

where ε_∞ denotes the optical dielectric constant, ε_s represents the static dielectric constant, ε_o corresponds to the vacuum dielectric constant, ω and τ represent angular frequency and polarization relaxation time.

$$\left(\varepsilon' - \frac{\varepsilon_s + \varepsilon_\infty}{2}\right)^2 + (\varepsilon'')^2 = \left(\frac{\varepsilon_s + \varepsilon_\infty}{2}\right)^2 \quad (5)$$

$$C_0 = \mu''(\mu')^{-2} f^{-1} \quad (6)$$

$$t_m = nc / 4 f_m (\varepsilon_r \mu_r)^{1/2} \quad (7)$$

where t_m denotes the matching thickness of the absorber, while λ represents the wavelength of the incident waves. The speed of light in vacuum is represented as c, and the corresponding matching frequency is denoted by f_m.

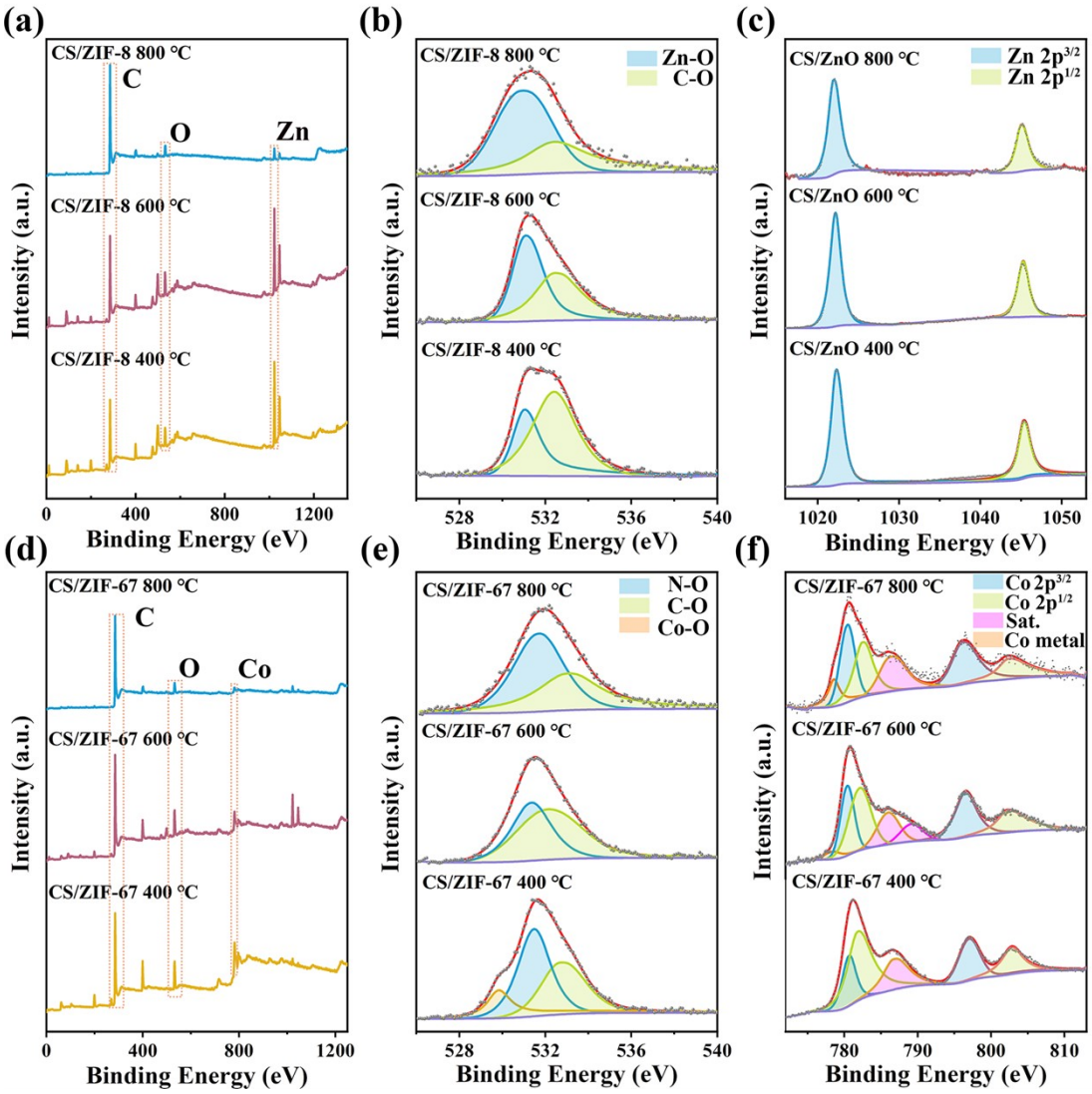

Fig. S1. (a, d) XPS survey spectra, (b, e) O 1s spectra and (c, f) Zn 2p and Co 2p for CS/ZIF-8 and CS/ZIF-67 at 400°C, 600°C and 800°C, respectively.

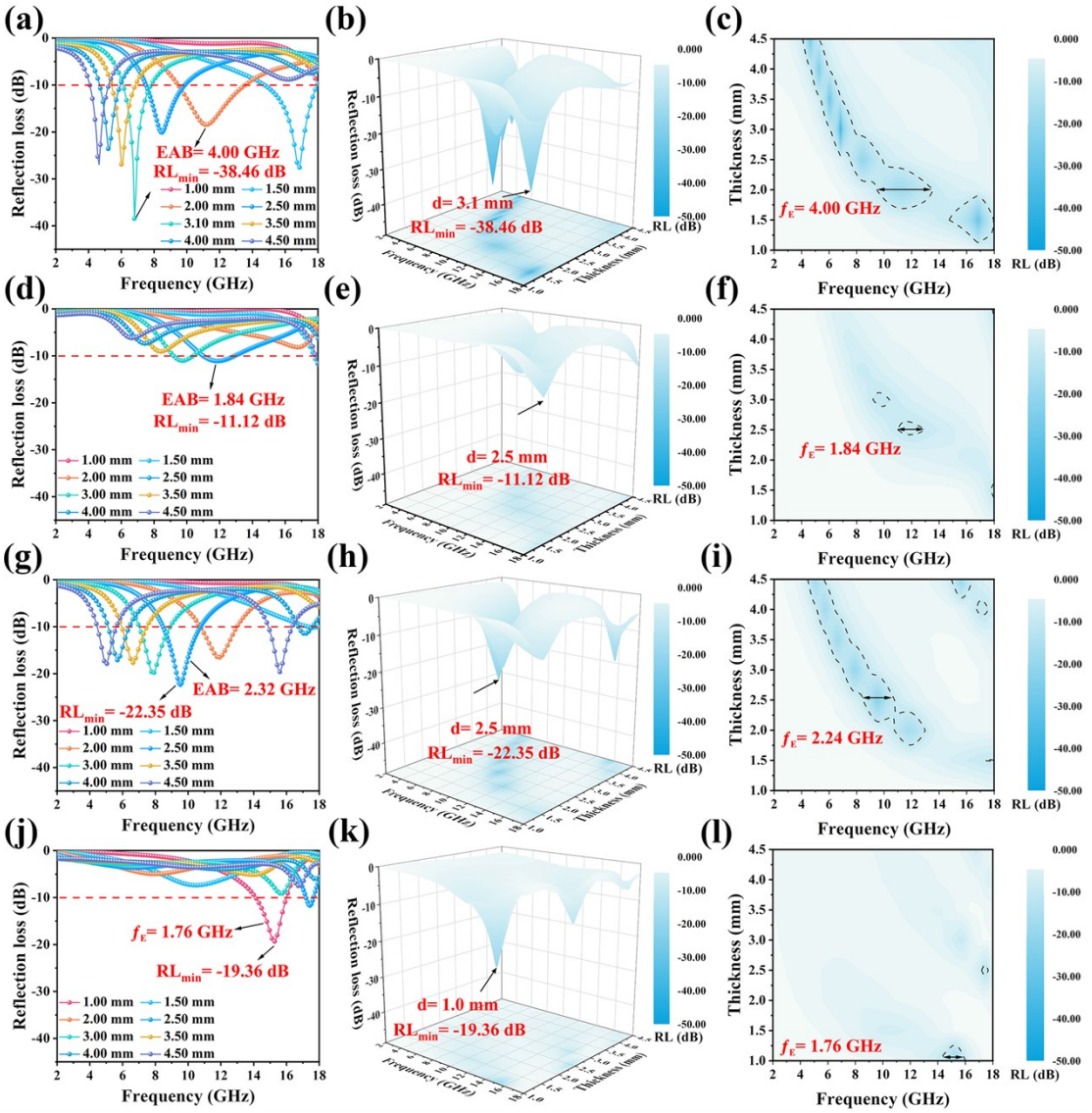

Fig. S2. 3D plots and 2D colored maps of RL values for (a-c) CS/ZIF-8 400℃, (d-f) CS/ZIF-8 800℃, (g-i) CS/ZIF-67 400℃ and (j-l) CS/ZIF-67 800℃.

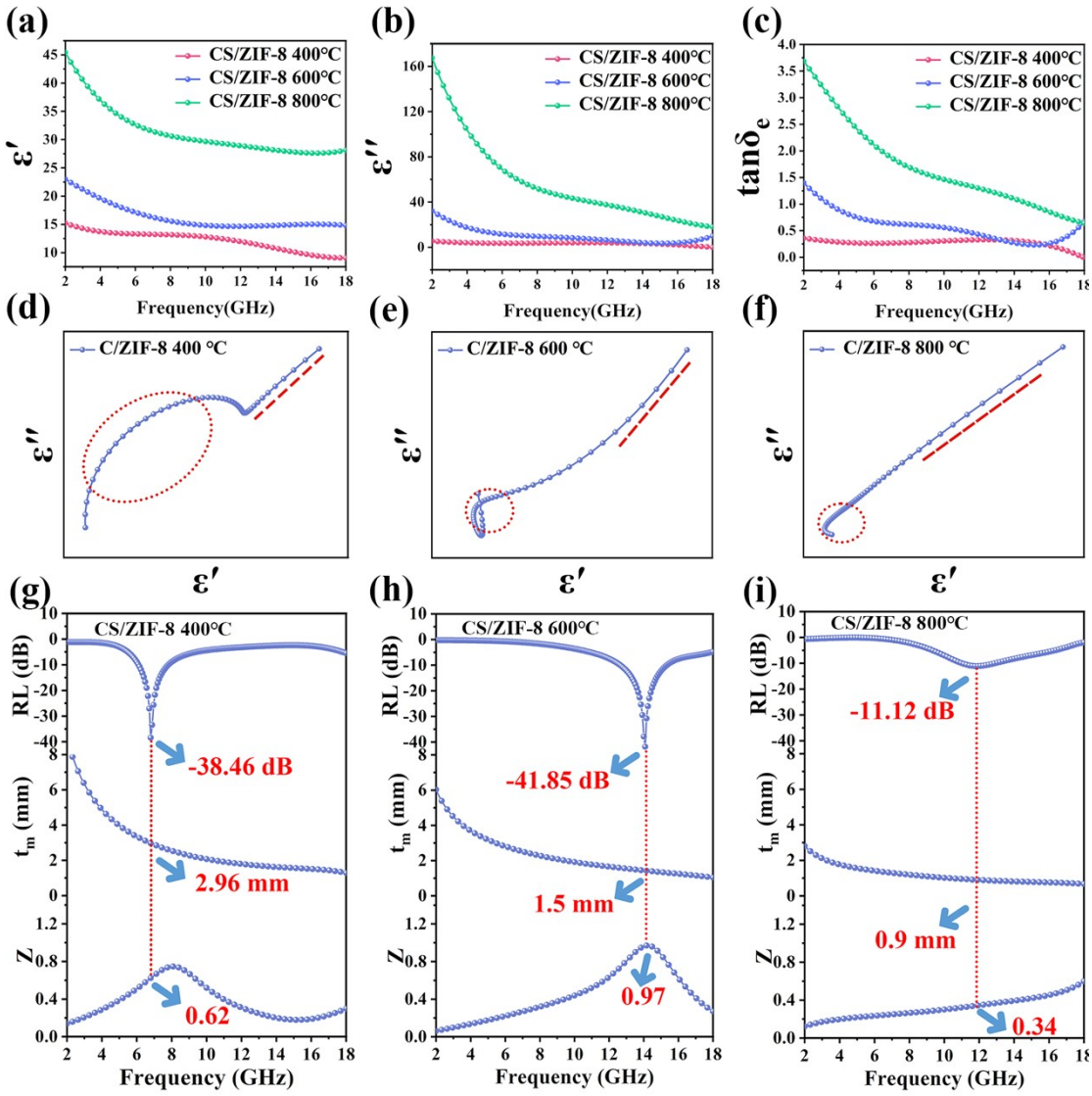

Fig. S3. The frequency-dependent behavior of (a) real parts ε', (b) imaginary parts ε'', (c) $\tan\delta_e$. (d–f) Cole-Cole plots, and (g–i) frequency dependence of RL, quarter wavelength (t_m), and normalized impedance $|Z_{in}/Z_0|$ for CS/ZIF-8.

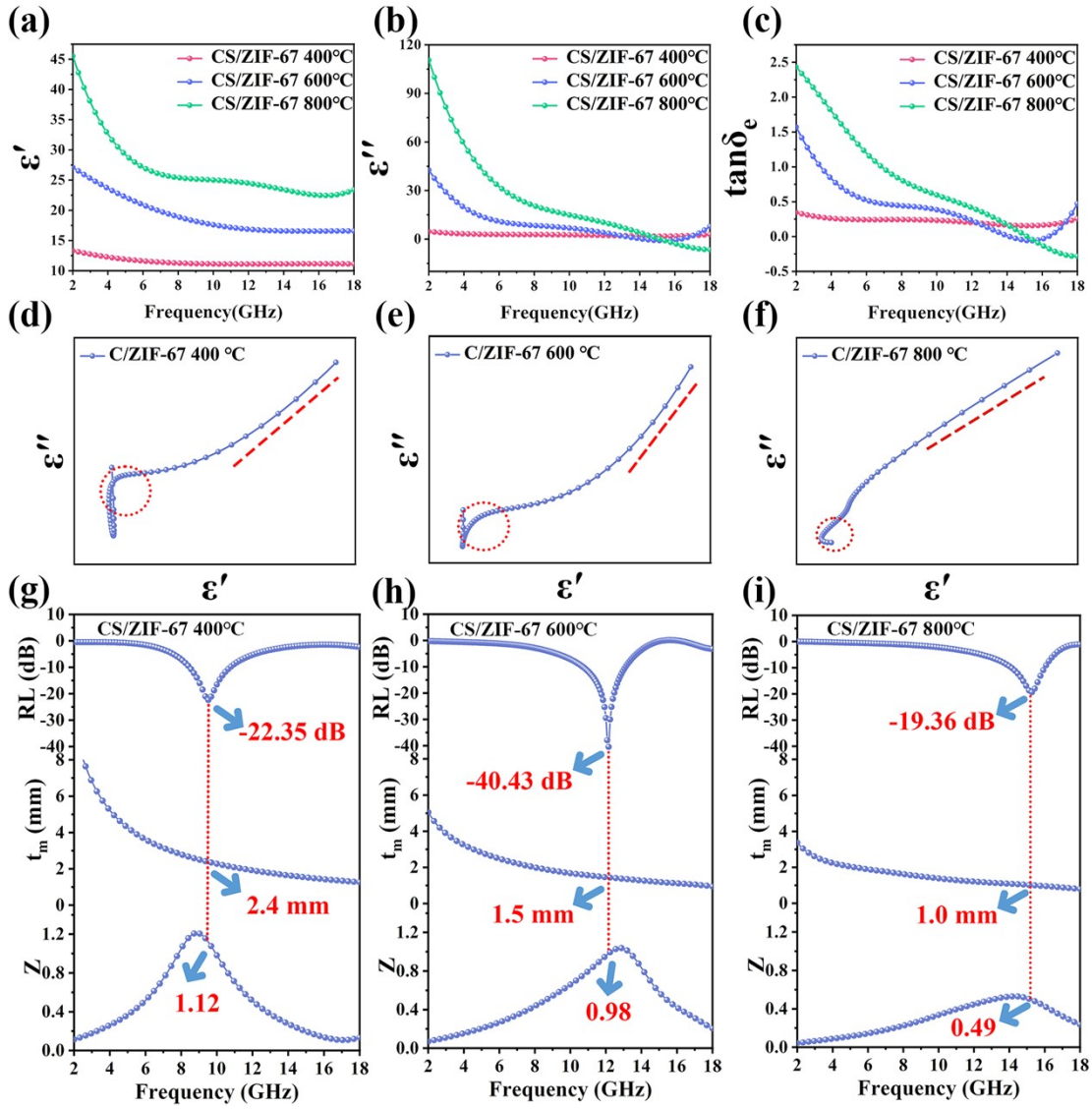

Fig. S4. The frequency-dependent behavior of (a) real parts ε', (b) imaginary parts ε'', (c) $\tan\delta_e$. (d–f) Cole-Cole plots, and (g–i) frequency dependence of RL, quarter wavelength (t_m), and normalized impedance $|Z_{in}/Z_0|$ for CS/ZIF-67.

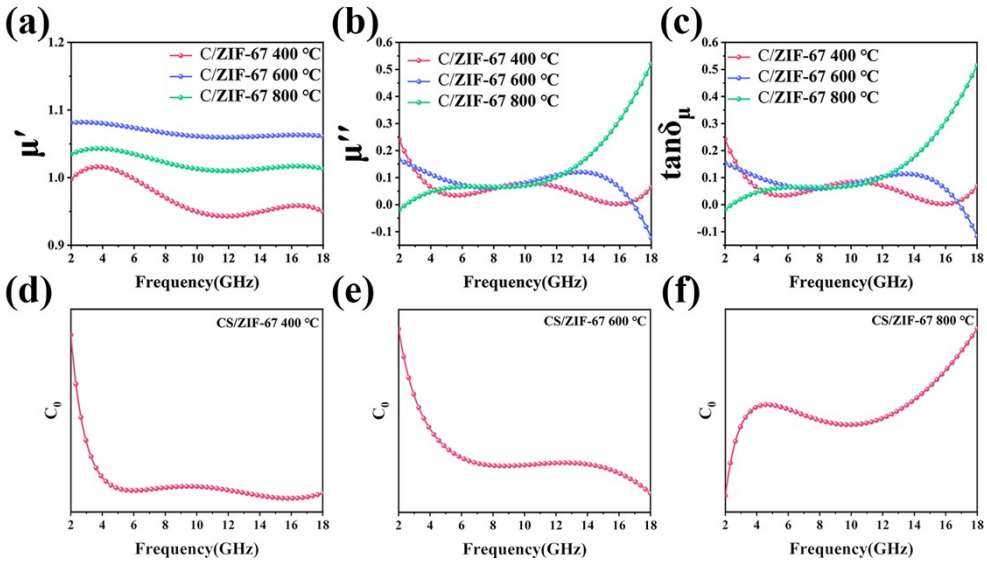

Fig. S5. The frequency-dependent behavior of (a) real parts μ', (b) imaginary parts μ'' and (c) $\tan\delta_{\mu}$. (d-f) C_0-f curves for CS/ZIF-67.

Fig. S6. Image of three-electrode system.

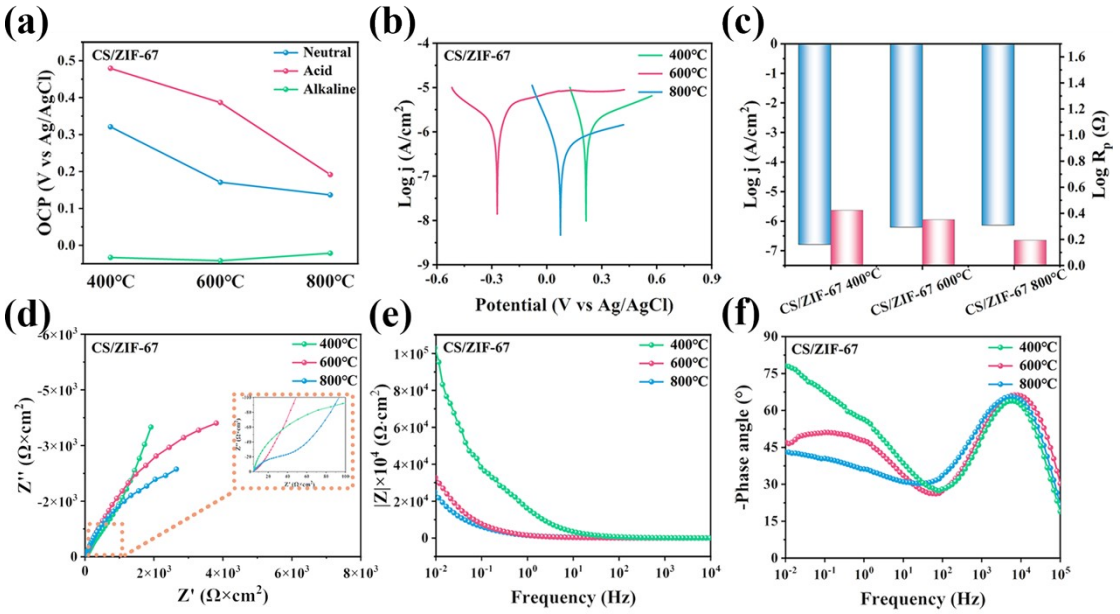

Fig. S7. (a) OCP values under acidic, neutral, and alkaline environments of CS/ZIF-67. (b) Tafel curves and (c) I_{corr} and R_p values in neutral corrosion conditions. (d) Nyquist plots (e) bode plots and (f) phase angle plots of absorbers in neutral solutions.